Direct-Write Assembly of 3D Silk/Hydroxyapatite Scaffolds for Bone Co-Cultures

*Lin Sun, Sara T. Parker, Daisuke Syoji, Xiuli Wang, Jennifer A. Lewis, and David L. Kaplan**

Three-dimensional (3D) microperiodic scaffolds composed of a gradient array of silk/hydroxyapatite (HA) filaments are fabricated by direct-write assembly. This approach allows for precise control over the printed filament size and location within each scaffold. These 3D silk/HA scaffolds are used to support the growth of co-cultures of human bone marrow derived mesenchymal stem cells (hMSCs) and human mammary microvascular endothelial cells (hMMECs) to assess *in vitro* formation of bone-like tissue. Histology reveals that the hMSCs and hMMECs form intricate networks of extracellular matrix within these 3D scaffolds. Vascular-like structures are only observed in co-cultures of hMSCs and hMMECs. When the spacing between silk/HA filaments is approximately 400 μm, the vascular-like structures follow the scaffold morphology. Direct writing of 3D scaffolds offers a novel route for investigating the effects of scaffold architecture and cell composition on human tissue formation.

There is a close connection between bone healing and blood vessel growth. In a fracture, damage to blood vessels induce a cascade of events, including the formation of a hemotoma and the recruitment of stem cells and fibroblasts to the wound site that trigger bone formation.[1] Bone formation requires adequate vascularization and inhibition of angiogenesis results in decreased bone mass.[2] In implant studies, bone vascular ingrowth *in vivo* is usually too slow to ensure the survival of graft and growth of new bone.[3] To understand the interaction between angiogenesis and osteogenesis as well as to construct pre-vascularized bone constructs *in vitro* for bone repair, a systematic approach to the interplay between vasculargenesis and osteogenesis is needed.

The properties of biomaterials play an important role in controlling cell attachment, alignment, proliferation, differentiation, and, ultimately, functional tissue generation. Besides chemical composition, which has been widely investigated, the physical properties of biomaterial scaffolding, such as geometry, pore size, porosity and connectivity, have significant effects on tissue regeneration.[4–6] For example, in osteogenesis, previous studies showed that honeycomb-shaped hydroxyapatite initiated higher bone formation than porous particles and porous blocks.[7] Pore size did not significantly affect osteogenesis *in vitro*, however new bone formation required larger pore sizes (>350 μm) for cell migration and angiogenesis *in vivo*.[5] As with osteogenesis, the size and shape of pores can affect vascularization. Smaller pores (5–20 μm) favor endothelial cell growth in vitro in 3D scaffolds,[8] while *in vivo* studies demonstrated that larger pores result in better vascularization. It was also found that 300–400 μm was the critical pore size above which caplillaries could be observed in newly formed bone.[9–12] Optimizing pore size is therefore essential for tissue studies *in vitro* and *in vivo*, and biomaterial scaffolds with controlled porosity gradients would be useful for the study of vascularized bone. Scaffolds with gradient pore sizes allow a side-by-side comparison of the impact of pore sizes, and also provide the possibility for formation of multiple types of tissues and tissue interfaces in one system, such as skeletal tissues composed of both vascularized bone and non-vascularized cartilage.

To investigate the effect of biomaterials architecture, including pore size and shape, on the bone tissue engineering from various materials, accurate control of scaffold fabrication is required. To date, many approaches have been reported, from porogen leaching and electrospun matrices, to micromolding and related techniques. One promising method relies on directly writing the biomaterial of interest at the microscale.[13,14] In this approach, a micronozzle is attached to a computer-controlled translation stage that moves in programmable 3D pattern and deposits the biomaterial ink only in desired locations. Various materials including poly(2-hydroxyethyl methacrylate) (pHEMA),[15] polyacrylic acid, (PAA), polyethylenimine (PEI)[13] have been used as ink solution in the direct writing technique.

Silk fibroin is a biomaterial that exhibits good biocompatibility, impressive mechanical strength, controllable degradation,

Dr. L. Sun, Prof. D. L. Kaplan
Department of Chemical and Biological Engineering and Biomedical Engineering
Tufts University
Medford, MA 02155, USA
E-mail: david.kaplan@tufts.edu
Dr. S. T. Parker, Dr. D. Syoji, Prof. J. A. Lewis
Department of Materials Science and Engineering
University of Illinois at Urbana-Champaign
Urbana, IL 61801, USA
Dr. X. Wang, Prof. D. L. Kaplan
Department of Biomedical Engineering
Tufts University
Medford, MA 02155, USA
Dr. X. Wang
Dalian Institute of Chemical and Physics
Chinese Academy of Sciences
116023, China

DOI: 10.1002/adhm.201200057

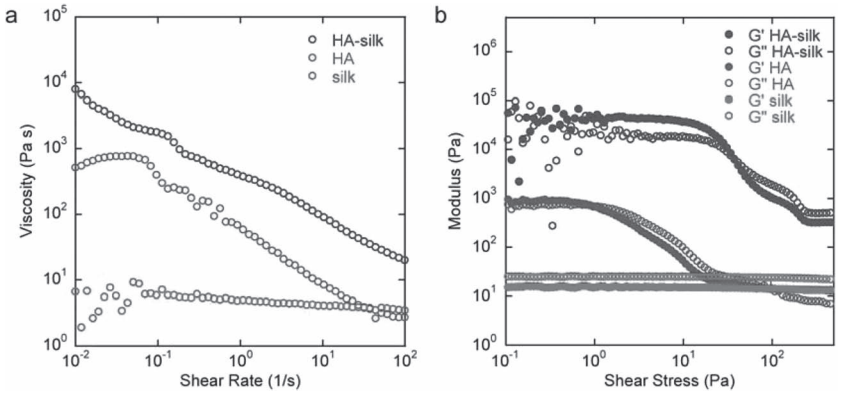

Figure 1. (a) Apparent viscosity as a function of shear rate for silk fibroin solution, HA suspension, and silk/HA ink. (b) Elastic (*G'*) and viscous (*G"*) moduli as a function of shear stress of these materials measured at an oscillation frequency of 1 Hz.

versatility in processing and modifications.[16–19] The use of silk as a supporting biomaterial for bone formation is documented both *in vitro* and in vivo.[20–24] Hydroxyapatite (HA) is a naturally occurring mineral in bone commonly termed apatite. It is commonly used for bone repair or ingrowth. Pre-mineralized silk scaffolds have been studied for bone formation[21,25,26] and the results suggested that mineralized porous scaffolds enhance osteogenesis from human bone marrow derived mesenchymal stem cells (hMSCs), resulting in better calcium deposition as a measure of more mature bone outcomes. However, increased mineralization also results in smaller pores and subsequently reduced transport, which can reduce cell ingrowth and function in the center of scaffolds, resulting in necrosis over time. Hence, further studies are needed to fully optimize pore sizes or porosity gradients for bone related tissue outcomes.

Here, we create a new silk fibroin ink filled with HA particles to print 3D scaffolds with gradient pore spacings ranging from 200 μm to 750 μm. Specifically, orthogonal periodic layers composed of silk/HA filaments (200 μm in diameter) are patterned in arrays with increasing spacing between each filament, to probe a variety of pore geometries on osteogenesis and vasculargenesis in one system. We first independently assessed osteogenesis with hMSCs and angiogenesis with hMMECs on these 3D silk/HA scaffolds, and then assessed co-cultures of these two cell types.

We first focused on designing a silk/HA ink with tailored rheological properties for printing 3D scaffolds with controlled pore architectures. This ink is created combining a silk fibroin solution with a concentrated HA suspension, whose respective rheological properties are shown in **Figure 1**. The silk solution exhibits nearly Newtonian behavior with a low shear viscosity of ~ 8 Pa•s and a plateau shear elastic modulus of roughly 10 Pa. By contrast, the HA suspension is a viscoelastic colloidal gel that exhibits a low shear apparent viscosity of ~ 600 Pa•s, strong shear thinning behavior and a plateau shear elastic modulus of nearly 10^3 Pa. Once combined, the silk/HA ink possesses an even higher apparent viscosity of ~ 10^4 Pa•s under low shear conditions and a plateau shear elastic modulus of nearly 10^5 Pa (Figure 1). Notably, this ink flows readily when extruded through a micronozzle (200 μm in diameter) under an applied pressure, yet quickly regains elasticity to maintain its filamentary shape upon exiting the nozzle.

Using this ink, silk/HA scaffolds are patterned by direct-write assembly in the form of a 3D lattice composed of interconnected silk/HA filaments with an interpenetrating gradient network of pore channels, whose spacing increases from 200 μm to 750 μm in increments of 50 μm across each printed layer. As a consequence, the scaffolds also contain a gradient in pore volume that increases from approximately 50 to 80%, respectively. An optical image of a representative silk/HA scaffold is shown in **Figure 2**a. Individual silk/HA filaments, imaged by scanning electron microscopy, span across underlying layers with little to no deformation (Figure 2b). Interestingly, the silk fibroin appears to promote bonding at each filament intersection. A higher magnification image of the surface of an individual filament (Figure 2c) reveals the presence of HA particles and the silk proteins that bind them together. The root-mean-square, surface roughness of the silk/HA filaments is 467 ± 61 nm, as determined by AFM (Figure 2d).

The silk/HA scaffolds have sufficient mechanical integrity to maintain their structure during the printing process, however it is necessary to strengthen them for cell culture experiments. Towards this objective, the scaffolds are immersed in a methanol-rich solution to promote the transformation of the silk proteins to the B-sheet conformation. Individual silk/HA filaments printed into a methanol-rich reservoir and dried exhibit an elastic module of 223 ± 9 MPa, which is three orders of magnitude higher than the shear elastic modulus of the silk/HA ink (0.1 MPa) and within an order of magnitude of methanol-treated electrospun silk-PEO blends (1300 MPa).[27]

The attachment and alignment of hMSCs were assessed on single layer of the scaffolds after 3 days and compared to cells grown on TCP (Figure S1). At day 3, hMSCs attached on both TCP and the silk/HA print surfaces. The cells showed star shapes and random orientations on the TCP (Figure S1b), while on the silk/HA scaffolds the hMSCS aligned along the direction of the rods and grew parallel within the spacings (Figure S1a).

Figure 3 shows that pores with characteristic sizes ranging from 200 to 750 μm are filled with cells and ECM after 6 weeks. Parallel cell strips formed between the patterned filaments and these strips have the same size as pores in which they are located within the 3D scaffolding. H&E staining confirmed cell attachment on silk/HA filaments. Cells grow on the printed filament surfaces and form tissue-like structures between them (Figure 3). More interestingly, organized swirl-like structures were observed within the ECM in the squares between adjacent filaments (Figure 3c), which resemble cell orientation in canals of human long bone.

To further evaluate the osteogenesis of hMSCs, bone specific markers including collagen type I, osteocalcin and mineralization are assessed by immunostaining, von Kosa and

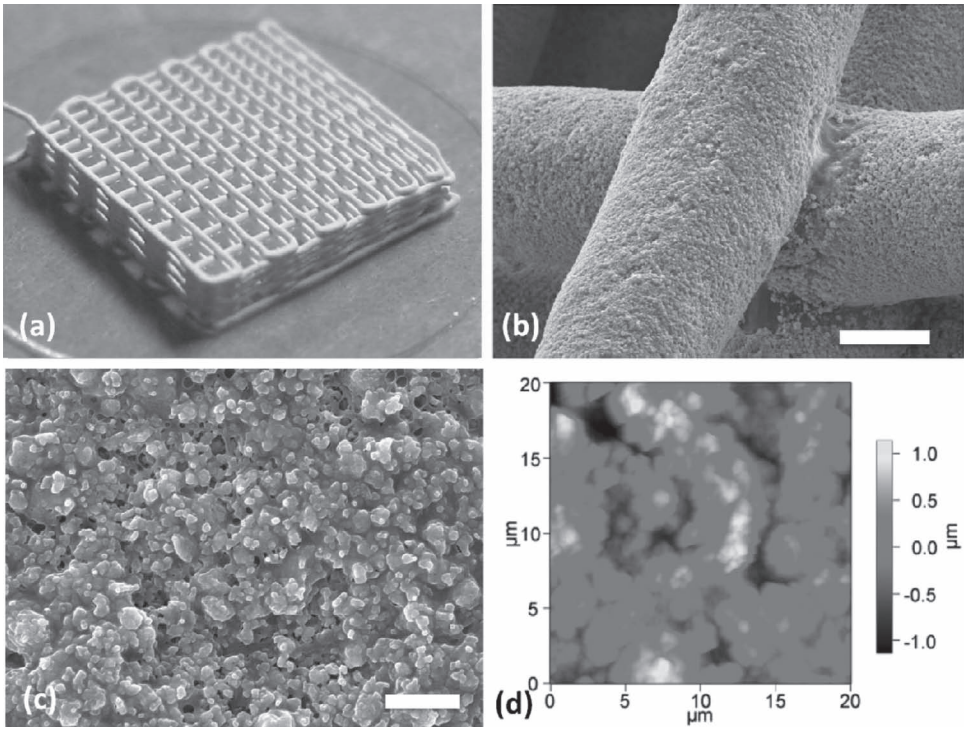

Figure 2. (a) Optical image of 3D silk/HA scaffold with gradient porosity, in which the largest (750 μm × 750 μm) and smallest (200 μm × 200 μm) pores are located at the bottom and top corners of the scaffold, respectively. (b) SEM image of printed silk/HA filaments intersecting between perpendicular layers. Sale bar, 100 μm. (c) Higher magnification view of the silk/HA filament surface. Scale, bar 10 μm. (d) Height profile of a representative silk/HA filament acquired by AFM.

SEM. **Figure 4** showed that after 6 weeks under osteogenic conditions, collagen type I accumulated throughout the scaffold within all pore spacings. Figure S2 confirmed cell growth and tissue formation based on H&E staining and further indicated mineral deposition by cells. However, no positive staining was found by Von Kossa or for osteocalcin. In future work, longer term cultures, hypoxia and the inclusion of BMP-2 may provide a more detailed assessment of osteogenesis, as has been shown in other studies.[7,19,28]

The morphology of endothelial cells in the silk/HA scaffolds was characterized by confocal microscopy. The cells were cobblestone shaped after seeding in the scaffolds (data not shown). At day 4, the cells filled the pores between adjacent silk/HA rods within the scaffold and attached to them from the smallest (200 μm) to largest (750 μm) sizes (**Figure 5**a,b). The first sign of small aggregates of aligned cells without identifiable lumens were observed within pores of all sizes. Moreover, in the medium pore size (400 μm), a complex interconnecting network of features with lumen-like structures are starting to form, observed both by phase-contrast mode (Figure 5d) and by live staining of the cells (Figure 5c).

The lumen-like structures formed by the endothelial cells have been shown previously in vitro in angiogenesis studies with different scaffolds, such as collagen, fibronectin, hyaluronan or Matrigel.[29–31] However, most *in vitro* work was performed on two-dimensional supports or hydrogels rather than the more rigid 3D scaffolds investigated here. We found network formation in these scaffolds within 10 days with a preference for a 400 μm pore size. *In vivo* studies have shown that vascular tissue advance into substrates faster as the pore diameter increased,[3] with a diameter of 250–300 μm found most effective for new vessel ingrowth among the pore sizes ranging from 20 μm to 300 μm.[28] However, there are no prior studies regarding the effect of pore sizes above 300 μm. hMSCs have been shown to support the formation of stable vascular tubes.[1,2,14] We observed similar results; tubular structures formed within all pore sizes evaluated. Further, cross-shape structures formed only at 400 μm spacing. Histology staining for CD 31 confirmed that the cross-shape structure had endothelial characteristics. However, more data is needed to determine if these features consist of a single cell type.

After 2 weeks culture, network-like structures are observed within co-cultures of hMMECs with hMSCs, features that are not present in monocultures of hMSCs (data not shown). In the hMMECS and hMSCS co-cultures, cross-shaped structures form only in regions with 400 μm pore sizes (red arrows in **Figure 6**a). To further characterize the structures, the endothelial specific marker CD31 was detected by immunostaining and observed on the cross shape body, providing evidence for a lumen-like feature of endothelial cells (Figure 6b). For other pores sizes, for example 750 μm, random network structures were observed by positive staining for CD 31 (Figure 6c).

3D HA/silk scaffolds with gradient pore size ranging from 200 μm to 750 μm were constructed by direct-write assembly. These silk/HA scaffolds offer significant advantages. First, this

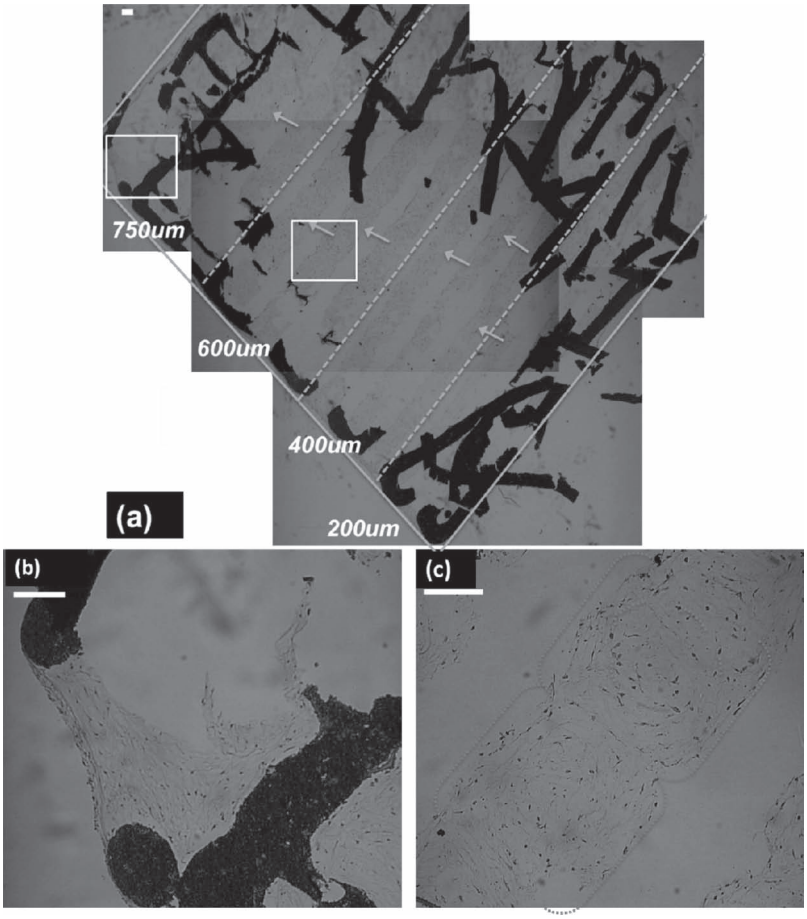

Figure 3. Histological evaluation of osteogenesis of hMSCs on silk/HA scaffolds at week 6. (a) Gross morphology of cells in the scaffold, scale bar. (b) cells attached along the rods and ECM formed, (c) cell patterns within strips. Scale bars = 100 µm.

patterning technique provides both versatility and the posibility of control over the scaffold composition, size, and architecture. These advantages can facilitate the study of angiogenesis and osteogenesis to optimize scaffold features. Second, by combining HA, a good matrix for hMSCs osteogenesis, with silk to promote endothelial cell growth and migration, we have created scaffolds capable of supporting both stem cell and endothelial cell functions to allow new tissue formation and bone remodeling with vascular inputs within a single construct environment.

The time of culture is important with respect to the formation of bone and vascular-like structures; hence, long-term studies using these 3D silk/HA scaffolds would be useful. One challenge identified in this work is that the number of cells present within features of varying pore size limits options for analysis. For example, within a given scaffold feature, few cells can be easily recovered for more extensive qPCR and related analyses. We therefore view these biomaterial constructs as a valuable initial screening tool to identify the most suitable pore size ranges/morphologies with which to pursue more detailed studies of tissue-related outcomes.

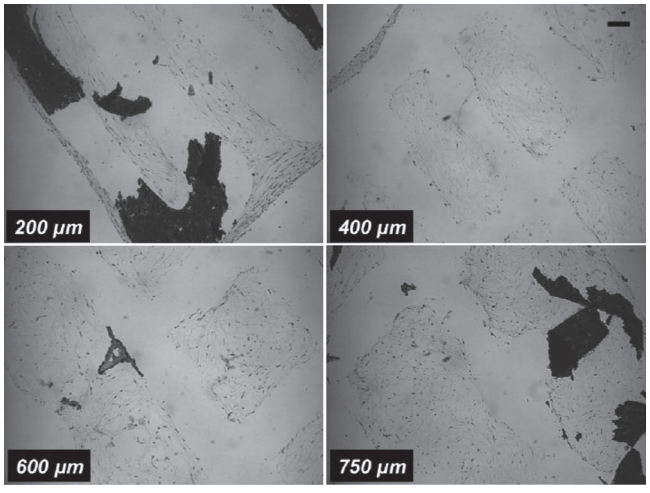

Figure 4. Immunohistology of collagen type I after 6 weeks. Scale bar = 100 µm for all images, spacing between adjacent silk/HA filaments is indicated in lower left of each image. The scaffolds also stained.

Experimental Section

Silk Fibroin Protein Purification: The silk protein was prepared as previously described.[16] Briefly, cocoons of *Bombyx mori* silkworm, supplied by Tajima Shoji Co. (Yokohama, Japan), are cut into pieces, and boiled in a Na_2CO_3 (0.02M) solution for 30 min. After boiling, degummed silk protein was rinsed thoroughly with distilled water and then dried overnight. The silk fibroin was dissolved in LiBr (9.3M) for 6 h at 60 °C to yield a 20% (w/v) silk solution. This solution was then transferred into Slide-a-Lyzer dialysis cassette (MWCO 3,500, Pierce) to dialyze against distilled water at room temperature. After 8 changes of water, a protein concentration of ~7–8% (w/v) was obtained.

Ink Preparation and Rheology: Commercially available hydroxyapatite (HA, $Ca_{10}(PO_4)_6(OH)_2$) particles (Lot#13310 Riedel-de Haen, Germany) were calcined at 1100 °C for 10 h and then ball milled at 30 rpm for 15 h. The resulting HA particles have a mean diameter of 2 um and a specific surface area of 3.8 m^2g^{-1}, as measured by centrifugal photo-sedimentation (Capa-700, Horiba Instruments Inc., Irvine, CA) and nitrogen adsorption (ASAP 2400 BET, Micrometrics, Norcross,GA), respectively.[32] A suspension was prepared by first dissolving the dispersant (Darvan 821, R.T.Vanderbilt Co., Norwalk,CT, a ammonium polyacrylic acid (PAA) solution (40 wt%)) in deionized water (0.57 g PAA m^2 HA^{-1}) and adjusting the pH to 9.0 (tuned with tetramethylammonium hydroxide (TMAH)(25 wt%) and nitric acid (HNO_3)(1M). Approximately half of the HA particles were added to the solution and mixed with a magnetic stir bar. This suspension was ultrasonicated (550 Sonic Dismembrator, Fisher Scientific, Pittsburgh, PA) for 10 min with 1 s on/off intervals and adjusted to pH 9.0. The remaining HA particles were added to the suspension, which was again ultrasonicated for 10 min and adjusted to pH 9.0. The suspension was then mixed with a magnetic stir bar for 12 h. The suspension was filtered (20 µm nylon net filter NY 2002500, Millipore, Billerica, MA) and centrifuged (Avanti J-25-I, Beckman Coulter, Brea, CA) at 2,000 rpm for 1 hr to concentrate it to nominally 40–45 vol% HA particles. To aggregate the stable suspension, polyethylene imine (10 wt%) (PEI, pH tuned to

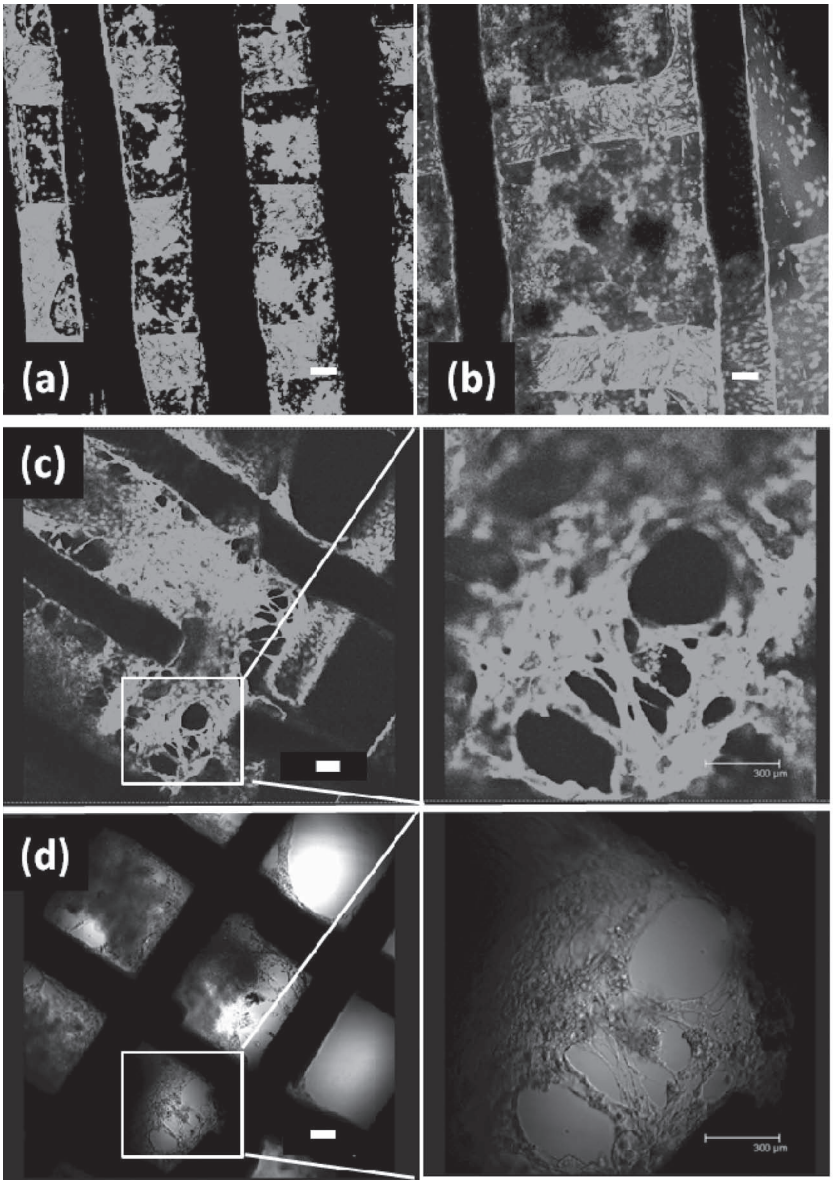

Figure 5. Morphology and viability of MMECs in silk/HA scaffolds at with characteristic pore sizes of (a) 200 μm, (b) 750 μm, and (c, d) 400 μm stained with live/dead. Live cells stained with calcein AM were green and dead cells stained with EthD-1 were red. Confocal microscopy images are acquired in fluorescence mode (c) and phase-contrast mode (d). Scale bar = 300 μm.

9.0, 600 g/mol branched, Polysciences, Inc., Warrington, PA) was added at a charge ratio of 0.5 [NHx]:[COO-] and, finally, the suspension was mixed with a Thinky planetary centrifugal mixer (ARE-250, Thinky, Tokyo, Japan) at 2000 rpm for 3 min.

The purified silk fibroin solution was diluted with pH 9.0 deionized water to a concentration of 3.89 wt%. This solution (~ 9 mL) was then dialyzed against a 15 wt% poly(ethylene glycol) (PEG) (8,000 g/mol, Sigma Aldrich, St. Louis, MO) solution at room temperature with Slide-a-Lyzer dialysis cassettes (MWCO 3,500). The volume ratio of PEG solution to silk fibroin solution was 40:1. After 14 h, the concentrated silk fibroin solution (~25–30 wt%) was slowly removed by a syringe to avoid excessive shearing. The ~40–45 vol% HA suspension was combined with the concentrated silk solution so that the silk:HA weight ratio was 1:9. This suspension was mixed with the Thinky mixer twice for 3 min each at 2,000 rpm. The suspension was dialyzed in the PEG solution for 50–60 min and removed by cutting open the dialysis cassettes. After dialysis, the final suspension was again mixed 3 times in the Thinky mixer at 2,000 rpm for 3 min, with the final mixing followed by a 3 min defoaming step at 2,000 rpm. This process yield a concentrated silk/HA ink composed of ~50 vol% of these two biomaterials.

The rheological properties of the silk/HA ink were measures using a controlled stress rheometer (Bohlin CVO Rheometer, Malvern Instruments Ltd., Worcestershire, UK) fitted with a cup and bob (coaxial cylinder) geometry (C8, bob diameter 8 mm). The apparent viscosity was measured as a function of shear rate and measurements were carried out in a logarithmically ascending series of discrete steps. The shear elastic shear (G') and viscous (G'') moduli were measured using an oscillatory technique, consisting of a logarithmic stress sweep at a frequency of 1 Hz. All measurements were carried out at 22 °C using a solvent trap filled with water to mitigate drying effects.

Scaffold Fabrication and Characterization: 3D silk/HA scaffolds were fabricated using a 3-axis micropositioning stage (ABL9000, Aerotech Inc., Pittsburgh, PA) controlled by customized software (3D Inks, Stillwater, OK). The ink was housed in a syringe (barrel diameter = 4.6 mm, EFD Inc., East Providence, RI) that was mounted on the x-y-z stage. The ink was extruded through a stainless steel 200 μm nozzle (EFD Inc.) onto a stationary glass substrate (15 mm diameter, #2 thickness, Electron Microscopy Sciences, Hatfield, PA). The ink was extruded under an applied pressure (800 Ultra dispensing system, EFD Inc., 275–350 kPa) at a constant deposition speed (2 mm s^{-1}). After patterning the initial layer, the nozzle was incrementally raised in the z-direction to generate the next layer. In each subsequent layer, an array of parallel filaments was printed such that their orientation was orthogonal to the layers immediately above and below a given layer. This process was repeated until the desired 3D scaffold was assembled. Gradient patterns were produced by increasing the distance between adjacent filaments from 200 μm to 750 μm in increments of 50 μm across each layer. The 8-layer scaffolds were printed with overall dimensions of approximately 8 mm × 8 mm × ~1.2 mm. To increase adhesion between each layer, the nozzle was incremented 150 μm along the z-axis between each layer.

After printing was complete, the scaffolds were placed in a closed container with methanol (MeOH, Sigma Aldrich) vapor for ~10 min. Increasing concentrations of 80%, 85%, 90%, and 100% by volume of MeOH/(MeOH + water) solutions were added to the scaffolds for ~10 min each and allowed to evaporate before the next solution was introduced. Each scaffold was then placed in another closed container with MeOH (80%)(MeOH + water) soaked into a paper wipe to allow for slow evaporation and avoid cracking. Scanning electron microscopy (SEM) images of 3D scaffolds were taken with a Hitachi S-4700 SEM (Hitachi Ltd., Tokyo, Japan). Prior to imaging, samples were coated with gold/palladium for 45 s (Emitech K575 Sputter Coater, Emitech Ltd., Ashford Kent, UK).

Dynamic mechanical analysis (DMA, TA Instruments, New Castle, DE) was carried out on silk/HA filaments formed by extruding the ink

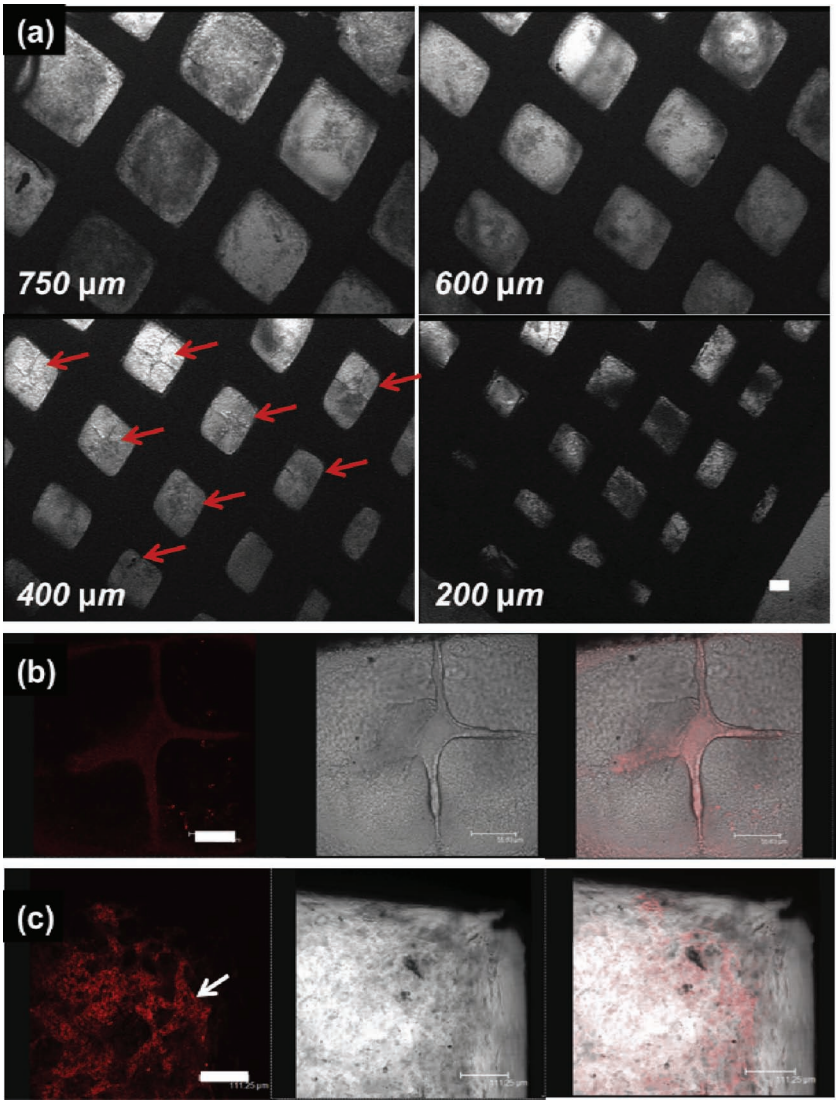

Figure 6. Morphology of co-cultures of hMMECs with hMSCs in silk/HA scaffolds at week 2. (a) Images taken under light field for all pore sizes. Scale bar = 100 µm for all Immunostaining of cells with CD 31 at 400 µm pore spacing (b) scale bar = 50 µm, and 750 µm spacing (c) Scale bar = 100 µm.

directly into 80% MeOH/(MeOH + water) solution. The filament was then removed, cut into a 15-20 mm long segment, loaded into a DMA fiber geometry with a 10 mm gap and measured at a frequency of 1 Hz. Atomic force microscopy (MFP-3D, Asylum Research, Santa Barbara, CA) was performed with a silicon tip (Tap300Al-G, Budget Probes, Sofia, Bulgaria) to measure the root-mean-square roughness of the printed silk/HA filaments.

Human Mesenchymal Stem Cell (hMSC) Culture: Fresh human bone marrow was obtained from Lonza (Basel, Switzerland), and hMSCs were isolated from fresh bone marrow, as described previously.[16] hMSCs were maintained and proliferated in culture medium, containing 90% high glucose DMEM, fetal bovine serum (FBS) (10%), penicillin, streptomycin (1%), fungizone antimycotic (PSF), non-essential amino acid (1%) (Invitrogen, Carlsbad, CA) and 1 ng/ml basic fibroblast growth factor (bFGF). When cells reached 80% confluence, they were detached with trypsin (0.25%) (Invitrogen, Carlsbad, CA) and replated or frozen (8% DMSO in culture medium). A total of 1×10^5 P2 cells were suspended in 100 µl and seeded in silk/HA scaffolds drop-wise. The scaffolds were incubated at 37 °C for 2 h for cell attachment before fresh media was supplied and replaced twice a week.

Osteogenesis with hMSCs: Silk/HA scaffolds were sterilized with 70% alcohol and UV light in a hood. After sterilization, they were incubated overnight in hMSC full culture medium (As described at 2.3) and then the medium was aspirated before cell seeding. P2 hMSCs were collected and suspended to a proper concentration and seeded into the scaffolds drop-wise, yielding 1×10^6 cells per print. Cells were incubated for 2 h before fresh medium was added. Osteogenesis medium contained alpha-minimum essential medium (αMEM) supplemented with 10% fetal bovine serum, penicillin (100 U ml^{-1}), streptomycin (100 µg ml^{-1}), amphotericin (0.25 µg ml^{-1}), non-essential amino acids (1%), beta-glycerol-2-phosphate (10 mM) (Sigma, St. Louis, MO), dexamethasone (100 nM) (Sigma, St. Louis, MO), and L-ascorbic acid (0.05 mM) (Sigma, St. Louis, MO). Medium was replaced twice a week. Samples were collected at week 6 for analysis of tissue-related outcomes.

hMMEC Culture: The human mammary microvascular endothelial cells (hMMECs) (ScienCell, Carlsbad, USA) at passage 5 were used to evaluate the capability of these 3D silk/HA scaffolds to support vascular cells. The hMMECs were cultured in endothelial growth medium (ECM) supplemented with FBS (5%), smooth muscle cell growth supplement (ECGS) (1%) and penicillin/streptomycin solution (P/S)(1%) (ScienCell Research Laboratories, Carlsbad, CA). Cultures were maintained in a humidified incubator at 37 °C and CO_2 (5%) and the medium was replaced every 2 days. Before seeding, each silk/HA scaffold was exposed to 40 ul of collagen I solution (50 ug ml^{-1}) for coating (BD Biosciences, Franklin Lakes, NJ USA), and then dried in a hood. 1×10^6 hMMECs were suspended in culture medium and seeded onto each scaffold in a drop-wise fashion. Cells were maintained at 37 °C for 2 h for attachment before fresh medium was added.

Co-culture of hMMECs and hMSCs: hMSCs and hMMECs were separately trypsinized and suspended in culture medium. 200 µl of a mixture of these two cells was prepared yielding 5×10^5 hMSCs and 1×10^6 hMMECs for each silk/HA scaffold. Before seeding, the scaffolds were briefly coated with type I collagen as described above. The co-culture medium consists of osteogenesis medium and ECM in a ratio of 1:2 (v/v). The culture was maintained in a humidified incubator at 37 °C and 5% CO_2 and the medium was replaced every 2 days.

Live/dead Staining: The viability of cells was examined by live/dead assay (Molecular Probes, Eugene, OR) following instructions from the manufacturer. Briefly, samples were washed with PBS, and incubated in 2 mM calcein AM (staining live cells) and 4 mM ethidium homodimer (EthD-1, staining dead cells) in PBS for 30 min at room temperature. Each scaffold was imaged by confocal laser scanning microscopy (CLSM; Leica SP2, Oberkochen, German). Images of a series of horizontal sections were acquired and combined in a z-stack with a depth of 200 µm.

Histological evaluation: Samples were washed with PBS and fixed in 4% formalin for histology staining. H.E and Von Kossa staining were conducted following routine protocols. Briefly, samples were dehydrated and embedded through a series of alcohols and paraffin. Sectioned scaffolds were stained with H&E (hematoxylin and eosin) and Von Kossa

dye (5% $AgNO_3$) separately, after rinsing off the extra dye, slides were rehydrated and sealed with cover slips.

Immunohistology: For immunofluorescence staining, samples fixed with cold ethanol were treated in an antigen-retrieval solution (Fisher, Pittsburgh, PA) for 15 min at 95 °C. After blocking with horse serum, samples were incubated with primary antibodies from mouse CD 31 (1:100 abcam MA). Negative controls were processed with the same procedures except incubation was with PBS buffer instead of the primary antibodies. FITC conjugated goat anti-mouse IgG (1:100; Sigma, St. Louis, MO) was used as the secondary antibody. All images were taken using confocal laser scanning microscopy (CLSM; Leica SP2, Oberkochen, German). Briefly, a 200 µm thickness of the scaffolds was chosen by setting the depth of the bottom and top, then 200 µm thicknesses were vertically sectioned into 10–20 even planes. Images taken for each plane were stack together to generate a z-stacked image.

Scanning Electron Microscopy (SEM): The morphology of seeded scaffolds was observed by SEM (Zeiss FESEM Supra55VP, Oberkochen, Germany). At particular time points, samples were harvested and fixed in 4% formaldehyde solution (Fisher, Houston, TX USA) for at least 24 h, then dehydrated through a series of ethanol gradients. Samples were coated with gold/palladium prior to SEM observation.

Supporting Information

Supporting Information is available from the Wiley Online Library or from the author.

Acknowledgements

This work was supported by the NSF DMR and CBET-0828028 and the NIH [P41 Tissue Engineering Resource Center P41 EB002520, EB003210 and AR005593] and the Air Force Office of Scientific Research. JAL, STP, and DS are supported by the NSF Nanoscale Science and Engineering Center for Directed Assembly of Nanostructures (Grant No. DMR-0642573).

Received: February 25, 2012
Revised: March 13, 2012
Published online: May 29, 2012

[1] J. M. Kanczler, R. O. Oreffo, *Eur. Cell Mater.* **2008**, *15*, 100.
[2] R. A. Carano, E. H. Filvaroff, *Drug Discov. Today* **2003**, *8*, 980.
[3] E. O. Johnson, T. Troupis, P. N. Soucacos, *Microsurgery* **2011**, *31*, 176.
[4] M. Rumpler, A. Woesz, J. W. Dunlop, J. T. van Dongen, P. Fratzl, *J. R. Soc. Interface* **2008**, *5*, 1173.
[5] V. Karageorgiou, D. Kaplan, *Biomaterials* **2005**, *26*, 5474.
[6] J. X. Lu, B. Flautre, K. Anselme, P. Hardouin, A. Gallur, M. Descamps, B. Thierry, *J. Mater. Sci. Mater. Med.* **1999**, *10*, 111.
[7] M. Frohlich, W. L. Grayson, L. Q. Wan, D. Marolt, M. Drobnic, G. Vunjak-Novakovic, *Curr. Stem Cell Res. Ther.* **2008**, *3*, 254.
[8] D. Narayan, S. S. Venkatraman, *J. Biomed. Mater. Res. A.* **2008**, *87*, 710.
[9] Y. Kuboki, Q. Jin, H. Takita, *J. Bone Joint Surg. Am.* **2001**, *83-A*, S105.
[10] E. Tsuruga, H. Takita, H. Itoh, Y. Wakisaka, Y. Kuboki, *J. Biochem.* **1997**, *121*, 317.
[11] W. Bonfield, *Philos. Transact. A Math Phys. Eng. Sci.* **2006**, *364*, 227.
[12] M. I. Santos, R. L. Reis, *Macromol. Biosci.* **2010**, *10*, 12.
[13] G. M. Gratson, M. Xu, J. A. Lewis, *Nature* **2004**, *428*, 386.
[14] S. Ghosh, S. T. Parker, X. Wang, D. L. Kaplan, J. A. Lewis, *Adv. Funct. Mater.* **2008**, *18*, 1883.
[15] J. N. Hanson Shepherd, S. T. Parker, R. F. Shepherd, M. U. Gillette, J. A. Lewis, R. G. Nuzzo, *Adv. Funct. Mater.* **2011**, *21*, 47.
[16] L. Meinel, V. Karageorgiou, S. Hofmann, R. Fajardo, B. Snyder, C. Li, L. Zichner, R. Langer, G. Vunjak-Novakovic, D. L. Kaplan, *J. Biomed. Mater. Res. A.* **2004**, *71*, 25.
[17] G. H. Altman, F. Diaz, C. Jakuba, T. Calabro, R. L. Horan, J. Chen, H. Lu, J. Richmond, D. L. Kaplan, *Biomaterials* **2003**, *24*, 401.
[18] Y. Wang, H. J. Kim, G. Vunjak-Novakovic, D. L. Kaplan, *Biomaterials* **2006**, *27*, 6064.
[19] P. C. Bessa, M. Casal, R. L. Reis, *J. Tissue Eng. Regen. Med.* **2008**, *2*, 81.
[20] J. H. Ye, Y. J. Xu, J. Gao, S. G. Yan, J. Zhao, Q. Tu, J. Zhang, X. J. Duan, C. A. Sommer, G. Mostoslavsky, D. L. Kaplan, Y. N. Wu, C. P. Zhang, L. Wang, J. Chen, *Biomaterials* **2011**.
[21] H. J. Kim, U. J. Kim, H. S. Kim, C. Li, M. Wada, G. G. Leisk, D. L. Kaplan, *Bone* **2008**, *42*, 1226.
[22] L. Meinel, O. Betz, R. Fajardo, S. Hofmann, A. Nazarian, E. Cory, M. Hilbe, J. McCool, R. Langer, G. Vunjak-Novakovic, H. P. Merkle, B. Rechenberg, D. L. Kaplan, C. Kirker-Head, *Bone* **2006**, *39*, 922.
[23] S. Sengupta, S. H. Park, A. Patel, J. Carn, K. Lee, D. L. Kaplan, *Tissue Eng. Part A.* **2010**, *16*, 3623.
[24] L. Sun, X. Wang, D. L. Kaplan, *Biomaterials* **2011**, *32*, 5581.
[25] C. Li, C. Vepari, H. J. Jin, H. J. Kim, D. L. Kaplan, *Biomaterials* **2006**, *27*, 3115.
[26] S. Bhumiratana, W. L. Grayson, A. Castaneda, D. N. Rockwood, E. S. Gil, D. L. Kaplan, G. Vunjak-Novakovic, *Biomaterials* **2011**, *32*, 2812.
[27] M. Wang, H.-J. Jin, D. L. Kaplan, G. C. Rutledge, *Macromolecules* **2004**, *37*, 6856.
[28] L. Wang, N. H. Dormer, L. F. Bonewald, M. S. Detamore, *Tissue Eng. Part A.* **2010**, *16*, 1937.
[29] S. M. Sweeney, C. A. Guy, G. B. Fields, J. D. San Antonio, *Proc. Natl. Acad Sci USA* **1998**, *95*, 7275.
[30] N. Fournier, C. J. Doillon, *Cell Biol Int Rep.* **1992**, *16*, 1251.
[31] A. de Mel, G. Jell, M. M. Stevens, A. M. Seifalian, *Biomacromolecules.* **2008**, *9*, 2969.
[32] J. L. Simon, S. Michna, J. A. Lewis, E. D. Rekow, V. P. Thompson, J. E. Smay, A. Yampolsky, J. R. Parsons, J. L. Ricci, *J. Biomed. Mater. Res. A* **2007**, *83*, 747.

